

# A THERMAL ELASTIC MODEL FOR CONSTRAINED CRYSTAL GROWTH WITH FACETS

JINBIAO WU\*, C. SEAN BOHUN<sup>†</sup>, AND HUAXIONG HUANG<sup>‡</sup>

**Abstract.** In this paper we present a model for computing thermal stress inside a crystal with facets. Using a systematical perturbation analysis, a semi-analytical thermal stress solution is obtained for constrained directional growth with small lateral heat flux. Our solution can be applied to crystals grown by various growth techniques such as the Czochralski method. The semi-analytical nature of the solution allows us to compute thermal stress in crystals with facets much more efficiently, compared to a full 3D simulation. Examples are given for crystals pulled in a variety of seed orientations.

**Key words.** Crystal growth, asymptotic expansion, anisotropy, facet formation, thermal stress, Czochralski technique.

**AMS subject classifications.** 74A10, 74F05, 74H10, 80A22, 82D25, 82D37, 65M06.

**1. Introduction.** Directional growth techniques such as the Czochralski (Cz) method are frequently used to produce high quality single crystals. Almost perfectly cylindrical crystals are grown for silicon and other semiconductor materials despite their internal structure and material anisotropy. For these crystals, the effect of material anisotropy on thermal stress has been investigated by assuming axisymmetric cylindrical shape [6, 20, 26, 27]. On the other hand, anisotropic effects such as facets are often visible on the surface of binary compound semiconductor crystals grown by these methods [18]. The effect of non-cylindrical shape on the thermal stress is therefore of practical interest.

In this paper, we extend a thermal stress model developed in [2] for axisymmetric crystals to anisotropic ones grown by directional growth techniques. Under the assumptions of weak lateral heat flux and anisotropic effects, we derive perturbation solutions for temperature and related thermal stress. As in [2], weak lateral heat flux is characterized by a small Biot number, which allow us to expand temperature into an asymptotic series and reduce a three-dimensional problem into a series of two-dimensional ones. When the anisotropic effect is weak, we can further convert these two-dimensional problems into a series one-dimensional (axisymmetric) ones. Similar expansions can be carried out for thermal stress and explicit solution can be obtained, based on one-dimensional temperature solutions. As a result, thermal stress can be computed without solving the thermal elastic equations which are originally three-dimensional in space.

To incorporate geometrical anisotropy into existing thermal stress models [2, 26], we need to predict facet formation and lateral crystal shape under growth constraints imposed by directional growth. While a significant amount of research on shape predictions has been carried out and documented in the literature (see [25] and references therein), much less attention has been paid to facet formation using directional growth

---

\*School of Mathematical Sciences, Peking University, Beijing, China 100871. [jwu@math.pku.edu.cn](mailto:jwu@math.pku.edu.cn)

<sup>†</sup>Faculty of Science, University of Ontario Institute of Technology, Oshawa, Ontario, Canada L1H 7K4. [sean.bohun@uoit.ca](mailto:sean.bohun@uoit.ca)

<sup>‡</sup>Department of Mathematics & Statistics, York University, Toronto, Ontario, Canada M3J 1P3. [hhuang@yorku.ca](mailto:hhuang@yorku.ca)

techniques. For directional growth, typically the lateral growth rate is given by

$$v_{\text{lateral}} = v_{\text{axial}} \tan(\theta - \theta_c) \quad (1.1)$$

where  $v_{\text{axial}}$  is the axial growth rate (rate of crystallization),  $\theta$  is the angle between the meniscus and the axial direction, and  $\theta_c$  is the contact angle between the crystal and the melt. In [24], a phenomenological model has been used for the contact angle

$$\theta_c = \bar{\theta}_c [1 + \alpha \cos(k\phi)] \quad (1.2)$$

where  $\bar{\theta}_c$  is the mean contact angle,  $\phi$  is the angle formed by the normal direction of the growth front and an intrinsic direction determined by the crystal structure,  $k$  is an integer, which is chosen in such a way to reflect certain symmetry (e.g.,  $k = 4$  for a cubic lattice structure), and  $\alpha$  is a parameter. For unconstrained growth, these types of models are commonly used to study pattern selection, morphological instability [8, 9, 12] as well as the growth of poly-crystals [25].

The model in [24] is useful when the primary interest is on facet formation of crystals grown by directional growth techniques. However, we must make a priori assumptions about the nature of the symmetry in the contact angle (based on surface energy). It is not clear how to estimate the relevant coefficients in those models which are consistent with material anisotropy as well as the complex interaction between the orientation of the crystal and its underlying lattice structure. In this paper, we propose a simple model for the lateral growth rate, which takes the following form

$$v_{\text{lateral}} = v_{\text{axial}} \min\{f(\mathbf{n} \cdot \mathbf{e}), \tan(\theta - \bar{\theta}_c)\} \quad (1.3)$$

where  $f(\cdot)$  is a given function of the angle formed by the normal direction of the lateral surface in the horizontal plane ( $\mathbf{n}$ ) and a reference direction ( $\mathbf{e}$ ). The characteristic function  $f(\cdot)$  is determined only by the lattice structure and pulling direction and is therefore consistent with the material anisotropy of the crystal. In other words, we assume that the ratio of the growth rate is determined by the crystal lattice structure unless the constraint for directional growth is active.

Using our growth model, we could predict facet formation and shape evolution during the entire growth process, starting from an arbitrary seed shape in any crystallographic orientation. Indeed, a perturbation solution for thermal stress is obtained following the growth model given in (1.3). However, computational results are only presented for idealized growth conditions where we fix the growth angle and assume an equilibrium lateral crystal shape, predicted by our model. This is due to the fact that our main objective of this paper is to investigate the effect of anisotropy on thermal stress instead of an exhausted study on shape evolution and facet formation using directional growth techniques.

The effect of anisotropy appears in two aspects: a geometric effect due to facet formation, and an intrinsic effect due to the anisotropy in the material (elastic) parameters of the crystal. In this paper we investigate the geometric effect while the combined geometric and material anisotropy case will be considered in a subsequent paper [28]. In Section 2 we will present a mathematical model for lateral growth and the thermal problem is described in Section 3. A perturbation solution for temperature is obtained in Section 4. In Section 5, we derive an expression for the thermal stress using isotropic elastic constants. Numerical results are presented in Section 6 for the  $[001]$ ,  $[\bar{1}\bar{1}\bar{1}]$  and  $[\bar{2}11]$  pulling directions<sup>1</sup> in the growth of a crystal with cubic

---

<sup>1</sup> $[\bar{h}\bar{k}l]$  denotes a unit vector in the  $\langle h, -k, l \rangle$  direction.

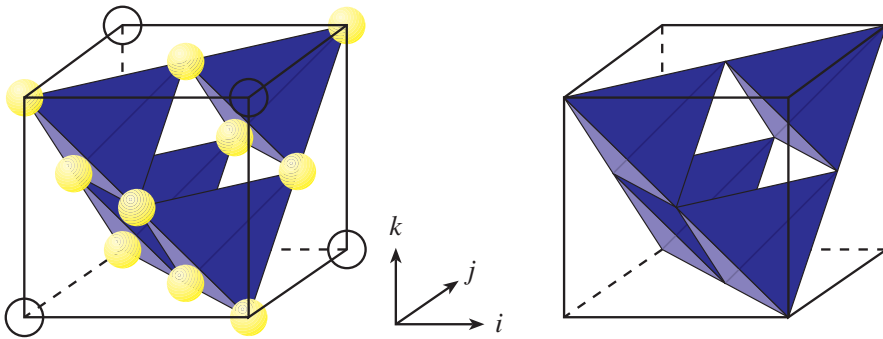


FIG. 2.1. Shown are the four tetrahedra of an AB unit cell. To the left only the B atoms in the unit cell are shown. B atoms in the unit cell but not included in the four growth units are represented with hollow circles. At the centre of each tetrahedral growth unit is a A atom accounting for all the atoms in the AB unit cell. On the right only the tetrahedra are shown.

symmetry. We finish the paper by summarizing our results and a briefly discussing future directions of research.

**2. Constrained Lateral Growth and Facet Formation.** Before one can determine the equilibrium shape of a given crystal one first needs to compute the growth rate as a function of the crystal orientation. Studies based solely on the crystal lattice geometry using the BFDH law and PBC energy methods [11] either make no consideration for the bond types or cannot explain the different growth rates between the positive and negative directions in a polar crystal such as the III-V semiconductors [16].

In order to include the polarity effects Zhong et al. [34, 35] suggested a coordination polyhedral growth unit model where the growth of the various crystal faces is related to the exposure of edges, angle, and planes of the anion-coordination polyhedra on these surfaces. The idea of representing the crystal structure in this manner predates the work of Zhong [1, 7, 21, 22, 23]. What is more recent is the concept of attributing the growth rate of a given crystal with the incorporation of these complexes rather than the incorporation of individual atoms. This idea has continued to develop in a series of recent papers [14, 15, 16, 17, 32, 33].

The important characteristic of the coordination polyhedra is that the element (face, edge, vertex) exposed at a given interface depends on its orientation. In this sense the growth rate of the various crystal faces are related to the element of the coordination polyhedron present at the interface. Quantitative growth rates can be obtained by noting that if a given polyhedron is an equilibrium shape, then the growth rate in any direction must be proportional to the thickness of a single shell of growth units added in that direction. For example, consider a two-dimensional unit square. If a layer of unit thickness is added to each of the faces and the resulting object remains a square then the growth rate of any vertex relative to the faces will be  $v_{\text{vertex}} = \sqrt{2}v_{\text{face}}$  and for any angle  $-\pi/4 \leq \theta \leq \pi/4$ , with  $\theta = 0$  corresponding to a face,  $v(\theta) = v_{\text{face}} \sec \theta$ . This simple idea can be generalized to other coordination polyhedron and it reflects the vertex, edge, face hierarchy noted above.

If we let AB denote a III-V semiconductor that belongs to the zinc-blende class of crystals then its anion-coordination polyhedra are the  $\text{AB}_4^{6-}$  tetrahedrons illustrated in Figure 2.1. By expressing the unit cell in terms of the tetrahedral growth units, the polarity of the III-V compounds naturally arise. The [111] (head) direction consists

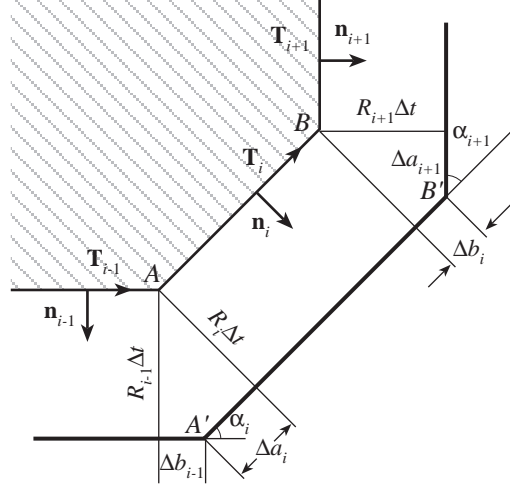


FIG. 2.2. Two-dimensional facet growth showing the relationship between the tangential and normal growth rates of related facets.

of exposed vertices and a fast growth rate whereas the  $[\bar{1}\bar{1}\bar{1}]$  (tail) direction consists of exposed faces and a slow growth rate.

If one considers Cz growth then the growth of the crystal is constrained to only those directions into the melt, and laterally, due to the meniscus supported at the crystal/melt interface. Indeed, to grow a cone with a  $1/2$  growing angle of  $\varphi$  we require

$$\tan \varphi = \frac{v_{\text{lateral}}(\mathbf{n})}{v_{\text{axial}}}$$

where  $\mathbf{n}$  denotes the lateral growth direction. However, since  $v_{\text{lateral}}(\mathbf{n})$  depends on the lateral direction, those directions where  $\tan^{-1}(v_{\text{lateral}}(\mathbf{n})/v_{\text{axial}}) \geq \varphi$  cannot be supported by the meniscus and will be truncated. Similarly, directions where  $\tan^{-1}(v_{\text{lateral}}(\mathbf{n})/v_{\text{axial}}) < \varphi$  will correspond to possible facets in the lateral direction. Following this, the growth angle  $\psi(\mathbf{n})$  is given by

$$\psi(\mathbf{n}) = \min \left\{ \varphi, \tan^{-1} \left( \frac{v_{\text{lateral}}(\mathbf{n})}{v_{\text{axial}}} \right) \right\}.$$

Starting with a circular seed, we evolve a two-dimensional cross-section corresponding to a lateral growth profile,  $v_{\text{lateral}}(\mathbf{n})$ , for a given pulling direction. The axial growth is in the opposite direction that the crystal is pulled and defines  $\psi(\mathbf{n})$ . Figure 2.2 illustrates the tangential growth rate of a given facet due to the relative orientation and normal growth rates of adjacent facets. From the figure, the tangential growth rate of the  $i$ th facet is given by

$$\begin{aligned} \frac{dl_i}{dt} &= \lim_{\Delta t \rightarrow 0} \frac{\Delta a_i + \Delta b_i}{\Delta t} = \frac{R_i \mathbf{n}_i \cdot \mathbf{n}_{i-1} - R_{i-1}}{\mathbf{T}_i \cdot \mathbf{n}_{i-1}} + \frac{R_{i+1} - R_i \mathbf{n}_i \cdot \mathbf{n}_{i+1}}{\mathbf{T}_i \cdot \mathbf{n}_{i+1}} \\ &= \frac{R_{i-1} - R_i \cos \alpha_i}{\sin \alpha_i} + \frac{R_{i+1} - R_i \cos \alpha_{i+1}}{\sin \alpha_{i+1}}. \end{aligned} \quad (2.1)$$

For the three characteristic directions  $[001]$ ,  $[\bar{1}\bar{1}\bar{1}]$  and  $[\bar{2}\bar{1}\bar{1}]$ , Figure 2.3 shows the constrained relative growth angle  $\psi(\mathbf{n})$  and the resulting equilibrium cross-sections

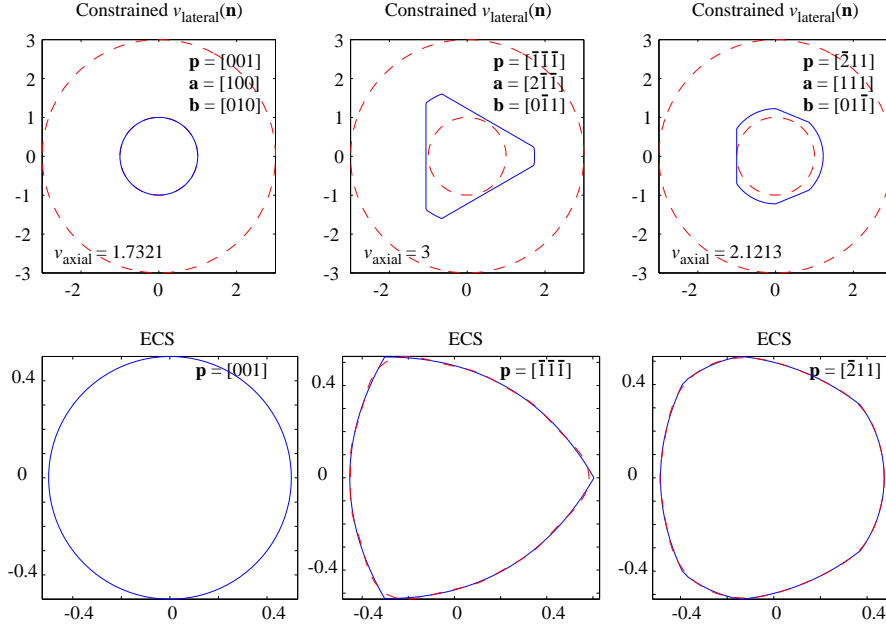


FIG. 2.3. Shown are the relative lateral growth rates  $v_{\text{axial}} \tan \psi(\mathbf{n}) = \min\{v_{\text{lateral}}, v_{\text{axial}} \tan \varphi\}$  and equilibrium cross-sections for the pulling directions  $\mathbf{p} = [001]$ ,  $[\bar{1}\bar{1}\bar{1}]$  and  $[\bar{2}11]$ . The vector  $-\mathbf{p}$  is directed into the melt and has the growth rate  $v_{\text{axial}}$ .  $\mathbf{a}$  and  $\mathbf{b}$  correspond to  $\phi = 0$  and  $\phi = \pi/2$  respectively. The curves  $r = 1$  and  $r = 3$  in plots of  $v_{\text{lateral}}$  respectively correspond to the growth rate in the face and vertex directions of the underlying growth units. In the simulation the contact angle is taken to be  $25^\circ$  corresponding to the III-V material InSb. The crystal is constrained to grow into a cone with a  $1/2$  opening angle of  $\varphi_{\text{cone}} = 5^\circ$ . Where discernible, the dashed curve in the ECS plots correspond to the data in Table 2.1. We note that our model produces crystals with shapes similar to those grown by our industrial partner [18].

(ECS) for a conic crystal grown with a  $1/2$  opening angle of  $\varphi_{\text{cone}} = 5^\circ$ . A representation of the ECS according to expression (3.2a) is tabulated in Table 2.1.

**3. Thermal Problem.** The basic assumptions of our model are that the lateral heat flux is small and the material and geometric anisotropic effects are weak. To simplify the discussion, we will assume that lateral heat transfer from the crystal to the background is known. In principle, we could incorporate the effect of the melt flow by coupling the heat transfer process in the crystal with that in the melt. However, to concentrate on the thermal stress in the crystal, we will neglect the effect of the melt flow and assume that the axial heat flux from the melt at the crystal/melt interface does not vary in the cross-sectional (radial and circumferential) directions.

Within the crystal  $\Omega$ , the temperature  $T(\mathbf{x}, t)$  satisfies the heat equation,

$$\rho_s c_s \frac{\partial T}{\partial t} = \nabla \cdot (\kappa_s \nabla T), \quad \mathbf{x} \in \Omega, \quad t > 0 \quad (3.1a)$$

where  $\rho_s$ ,  $c_s$  and  $k_s$  are the density, specific heat, and thermal conductivity of the crystal. The boundary conditions are below,

$$-\kappa_s \frac{\partial T}{\partial \mathbf{n}} = h_{\text{gs}}(T - T_g) + h_F(T^4 - T_b^4), \quad \mathbf{x} \in \Gamma_g, \quad (3.1b)$$

$$\kappa_s \frac{\partial T}{\partial z} = h_{\text{ch}}(T - T_{\text{ch}}), \quad z = 0, \quad (3.1c)$$

TABLE 2.1

Parameters corresponding to expression (3.2a) for the equilibrium cross-sections illustrated in Figure 2.3. In all cases  $n_k = k$ ,  $m = 10$  and  $\delta_k = 0$ . The results are obtained by starting with a circular seed with 1200 facets and computing an FFT on the final shape with  $N = 262144$  points.

$k$	$\beta_k : \mathbf{p} = [001]$ $\alpha = 0.00083$	$\beta_k : \mathbf{p} = [111]$ $\alpha = 0.12313$	$\beta_k : \mathbf{p} = [211]$ $\alpha = 0.08918$
1	1.00000	0.00003	-0.66503
2	0.00023	0.00004	-0.22615
3	0.00002	0.95149	0.63239
4	0.00002	0.00001	-0.29841
5	0.00002	0.00002	-0.11419
6	0.00002	0.27930	0.02665
7	0.00002	0.00001	-0.03487
8	0.00002	0.00002	0.04491
9	0.00002	0.12903	-0.00703
10	0.00002	0.00001	0.02444

where  $h_{gs}$  and  $h_{ch}$  represent the heat transfer coefficients;  $h_F$  the radiation heat transfer coefficient;  $T_g$ ,  $T_{ch}$  and  $T_b$  denote the ambient gas temperature, the chuck temperature and background temperature respectively.

The crystal/melt interface is denoted  $\Gamma_S$  and is where  $T = T_m$ , the melting temperature. Explicitly we denote the melting isotherm by

$$z - S(\mathbf{x}, t) = 0, \quad \mathbf{x} \in \Gamma_S. \quad (3.1d)$$

The motion of the interface of the phase transition is governed by the Stefan condition

$$\rho_s L |\mathbf{v}_n| = \kappa_s \left. \frac{\partial T}{\partial \mathbf{n}} \right|_{z \rightarrow S^-} - q_{l,n}, \quad |\mathbf{v}_n| = v_n = \frac{\partial S}{\partial t} \mathbf{k} \cdot \mathbf{n} \quad (3.1e)$$

where  $L$  is the latent heat,  $|\mathbf{v}_n|$  is the speed of the interface in the direction of its outward normal  $\mathbf{n}$ , and  $q_{l,n}$  is the heat flux from the melt normal to the interface. The speed  $\partial S / \partial t$  is the speed of the interface  $S$  in the  $\mathbf{k}$  direction.

**3.1. Crystal shape.** For the purpose of computing thermal stress, we assume the following expression in the case of weak anisotropy ( $\alpha$  small)

$$R(\phi, z) = \bar{R}(z) \left( 1 + \alpha \sum_{k=1}^m \beta_k \cos(n_k \phi + \delta_k) \right) = \bar{R}(z) (1 + \alpha \lambda(\phi)), \quad (3.2a)$$

where  $m$ ,  $n_1 < n_2 < \dots < n_m$  are positive integers ( $m = 1, n_1 = 4$  for four-fold symmetry) and  $\delta_k, \beta_k$  are constants with  $\sum_{k=1}^m \beta_k^2 = 1$ . In other words, we assume that the lateral shape of the crystal is in equilibrium with coefficients given in Section 2 for the three pulling directions being considered in this paper. Of particular interest are the angular integrals

$$I_{i,j}(\alpha) = \int_0^{2\pi} (1 + \alpha \lambda)^i \left( (1 + \alpha \lambda)^2 + (\alpha \lambda')^2 \right)^{j/2} d\phi \quad (3.2b)$$

where  $i, j \in \mathbb{Z}$ . From the choice of  $\lambda$ ,

$$\int_0^{2\pi} \lambda d\phi = 0, \quad \int_0^{2\pi} \lambda^2 d\phi = \pi, \quad \int_0^{2\pi} (\lambda')^2 d\phi = \pi \sum_{k=1}^m n_k^2 \beta_k^2,$$

and as a result,

$$I_{i,j}(\alpha) = 2\pi + \frac{\pi}{2} \left[ (i+j)(i+j-1) + j \sum_{k=1}^m n_k^2 \beta_k^2 \right] \alpha^2 + O(\alpha^3). \quad (3.2c)$$

Both the enclosed area ( $A$ ) and circumference ( $s$ ) of  $R$  will be utilized in the sequel. For any fixed  $z$  it is an easy exercise to verify  $A(z) = \bar{R}^2 I_{2,0}/2$  and  $s(z) = \bar{R} I_{0,1}$ .

**3.2. Non-dimensionalization.** For simplicity, we assume that the gas temperature  $T_g$  is constant. Defining the Biot number by

$$\epsilon = \frac{\bar{h}_{\text{gs}} \tilde{R}}{\kappa_s} \quad (3.3)$$

where  $\tilde{R}$  is a characteristic radius of the crystal and  $\bar{h}_{\text{gs}}$  is the mean value of  $h_{\text{gs}}$ . We adopt the following scalings:

$$\begin{aligned} r &= \tilde{R} \hat{r}, & R(\phi, z) &= \tilde{R} \hat{R}(\hat{\phi}, \hat{z}), & \epsilon^{1/2} z &= \tilde{R} \hat{z}, & \epsilon^{1/2} S(r, \phi, t) &= \tilde{R} \hat{S}(\hat{r}, \hat{\phi}, \hat{t}), \\ \text{St} &= \frac{L}{c_s \Delta T}, & \Delta T &= T_m - T_g, & T &= T_g + \Delta T \Theta, & t &= \frac{\text{St} \tilde{R}^2 \rho_s c_s}{\kappa_s \epsilon} \hat{t}, \end{aligned}$$

with  $\phi = \hat{\phi}$ . Here variables with hats ( $\hat{\cdot}$ ) are the non-dimensional ones. In terms of these variables the heat equation (3.1a) becomes

$$\frac{\epsilon}{\text{St}} \Theta_t = \frac{1}{r} (r \Theta_r)_r + \frac{1}{r^2} \Theta_{\phi\phi} + \epsilon \Theta_{zz}, \quad \mathbf{x} \in \Omega, t > 0, \quad (3.4a)$$

with boundary conditions (3.1b)-(3.1d)

$$-\Theta_r + \frac{1}{R^2} R_{\phi} \Theta_{\phi} + \epsilon R_z \Theta_z = \epsilon F(\Theta) \left( 1 + \frac{R_{\phi}^2}{R^2} + \epsilon R_z^2 \right)^{1/2}, \quad \mathbf{x} \in \Gamma_g, \quad (3.4b)$$

$$\Theta_z(0, \phi, t) = \delta (\Theta(0, \phi, t) - \Theta_{\text{ch}}), \quad (3.4c)$$

$$\Theta = 1, \quad \mathbf{x} \in \Gamma_S, \quad (3.4d)$$

where

$$F(\Theta) = \frac{h_F(T_g^4 - T_b^4)}{h_{\text{gs}} \Delta T} + \left( \beta(z) + \frac{4h_F T_g^3}{h_{\text{gs}}} \right) \Theta + \frac{h_F}{h_{\text{gs}}} \Delta T (6T_g^2 + 4T_g \Delta T \Theta + \Delta T^2 \Theta^2) \Theta^2,$$

$\beta(z) = h_{\text{gs}}/\bar{h}_{\text{gs}}$ , and  $\delta = \epsilon^{1/2} h_{\text{ch}}/\bar{h}_{\text{gs}}$ . The hats have been dropped for brevity. The crystal/melt interface advances according to the Stefan condition (3.1e) which in non-dimensional co-ordinates becomes

$$\Theta_z - \frac{1}{\epsilon} S_r \Theta_r - \frac{1}{\epsilon r^2} S_{\phi} \Theta_{\phi} = \gamma + S_t, \quad \gamma = \frac{q_l \tilde{R}}{\epsilon^{1/2} \kappa_s \Delta T}, \quad (3.4e)$$

where  $\gamma$  ( $q_l$ ) is the non-dimensional (dimensional) heat flux in the liquid across the crystal/melt interface in the axial direction.

**4. Temperature Solution.** Much of the asymptotic framework discussed in this paper has appeared elsewhere in the literature [2, 5, 10, 13, 29, 30, 31] in an axis-symmetric case. Kuiken and Roksnoer [13] obtained an accurate temperature distribution for a Si crystal grown with the floating-zone technique. By using an expansion in terms of the Péclet and Nusselt numbers of the crystal, they obtained a solution valid for slender crystals grown in conductive heat transfer environments. An asymptotic analysis that considered the melt was undertaken by Brattkus and Davis [5], where the geometry allowed an expansion in terms of the aspect ratio of the solidification cell. Young and Chait [29] considered a system driven by surface tension and more recently Young and Heminger [30, 31] have utilized a small aspect ratio to study the growth of single crystal fibres.

Equations (3.4a) and (3.4b) strongly suggest that the temperature  $\Theta$  is independent of  $r$  and  $\phi$  to leading order. If true then the crystal/melt interface  $S$  is also independent of  $r$  and  $\phi$  to leading order. These observations motivate the following expansions:

$$\begin{aligned}\Theta &\sim \Theta_0(z, t) + \epsilon\Theta_1(r, \phi, z, t) + \epsilon^2\Theta_2(r, \phi, z, t) + \dots, \\ S &\sim S_0(t) + \epsilon S_1(r, \phi, t) + \epsilon^2 S_2(r, \phi, t) + \dots.\end{aligned}\quad (4.1)$$

We substitute them into the scaled model, expand in powers of  $\epsilon$ , simplify and collect terms of the same orders. The resulting field equations to first order are:

$$\frac{1}{St}\Theta_{j,t} - \Theta_{j,zz} = \frac{1}{r}(r\Theta_{j+1,r})_r + \frac{1}{r^2}\Theta_{j+1,\phi\phi}, \quad \mathbf{x} \in \Omega, \quad t > 0, \quad j = 0, 1, \quad (4.2)$$

where the boundary condition on the lateral surface becomes

$$\left( \Theta_{1,r} - \frac{1}{R^2}R_\phi\Theta_{1,\phi} - R_z\Theta_{0,z} + F(\Theta_0) \left( 1 + \frac{R_\phi^2}{R^2} \right)^{1/2} \right) (R(\phi, z), \phi, z, t) = 0, \quad (4.3a)$$

$$\begin{aligned}\left( \Theta_{2,r} - \frac{1}{R^2}R_\phi\Theta_{2,\phi} - R_z\Theta_{1,z} + F'(\Theta_0)\Theta_1 \left( 1 + \frac{R_\phi^2}{R^2} \right)^{1/2} \right. \\ \left. + \frac{1}{2}R_z^2F(\Theta_0) \left( 1 + \frac{R_\phi^2}{R^2} \right)^{-1/2} \right) (R(\phi, z), \phi, z, t) = 0.\end{aligned}\quad (4.3b)$$

Continuing this procedure for the remaining conditions, at the top of the crystal one has

$$\Theta_{0,z}(0, t) = \delta(\Theta_0(0, t) - \Theta_{\text{ch}}), \quad (4.4a)$$

$$\Theta_{1,z}(r, \phi, 0, t) = \delta\Theta_1(r, \phi, 0, t), \quad (4.4b)$$

and at the solid-liquid interface

$$\Theta_0(S_0(t), t) = 1, \quad (4.5a)$$

$$(S_1\Theta_{0,z} + \Theta_1)(r, S_0(t), t) = 0. \quad (4.5b)$$

Finally, the evolution of the interface is governed by

$$S'_0(t) = \Theta_{0,z}(S_0(t), t) - \gamma, \quad S_0(0) = Z_0, \quad (4.6a)$$

$$S_{1,t}(r, \phi, t) = \left( \Theta_{1,z} + S_1\Theta_{0,zz} + \frac{\Theta_{1,r}^2}{\Theta_{0,z}} + \frac{\Theta_{1,\phi}^2}{r^2\Theta_{0,z}} \right) \Big|_{z=S_0(t)}, \quad S_1(r, \phi, 0) = 0. \quad (4.6b)$$

Here  $Z_0$  is the non-dimensional length of the seed.

**4.1. Solution of the zeroth order model.** Let  $\Delta_{r\phi}$  denote the two-dimensional Laplacian operator in  $(r, \phi)$  so that (4.2) with  $j = 0$  and (4.3a) can be written as

$$\Delta_{r\phi}\Theta_1 = \frac{1}{\text{St}}\Theta_{0,t} - \Theta_{0,zz}, \quad \mathbf{x} \in \Omega, \quad t > 0, \quad (4.7a)$$

$$\frac{\partial\Theta_1}{\partial\mathbf{n}_{r\phi}} = -F(\Theta_0) + R_z\Theta_{0,z} \left(1 + \frac{R_\phi^2}{R^2}\right)^{-1/2}, \quad r = R(\phi, z). \quad (4.7b)$$

Here  $\mathbf{n}_{r\phi}$  is the unit normal vector in the cross-section. A necessary condition for the existence of  $\Theta_1$  is that

$$\iint_{A(z)} \left(\frac{1}{\text{St}}\Theta_{0,t} - \Theta_{0,zz}\right) dA = \int_{s(z)} \left(-F(\Theta_0) + \frac{R_z\Theta_{0,z}}{\left(1 + \frac{R_\phi^2}{R^2}\right)^{1/2}}\right) ds$$

or

$$\left(\frac{1}{\text{St}}\Theta_{0,t} - \Theta_{0,zz}\right) \frac{\bar{R}^2 I_{2,0}}{2} = \bar{R}\bar{R}'I_{2,0}\Theta_{0,z} - \bar{R}I_{0,1}F(\Theta_0) \quad (4.8)$$

using (3.2). Combining (4.8) and the earlier results gives the zeroth order problem<sup>2</sup>

$$\frac{1}{\text{St}}\Theta_{0,t} - \Theta_{0,zz} = \frac{2}{R} \left(\bar{R}'\Theta_{0,z} - \frac{I_{0,1}}{I_{2,0}}F(\Theta_0)\right), \quad 0 < z < S_0(t), \quad t > 0, \quad (4.9a)$$

$$\Theta_{0,z}(0, t) = \delta(\Theta_0(0, t) - \Theta_{\text{ch}}), \quad t \geq 0, \quad (4.9b)$$

$$\Theta_0(S_0(t), t) = 1, \quad t \geq 0, \quad (4.9c)$$

$$S_0'(t) = \Theta_{0,z}(S_0(t), t) - \gamma, \quad S_0(0) = Z_0, \quad t > 0. \quad (4.9d)$$

**4.2. Solution of the first order model.** With respect to the Neumann problem (4.7a)-(4.7b), in general, numerical methods need to be used to solve for  $\Theta_1$ . However, in the case of weak anisotropy, i.e.,  $\alpha \ll 1$  in (3.2a), an approximate first order model can be derived. Denote

$$\Theta_1^*(r, \phi, z, t) = \Theta_1(r, \phi, z, t) - \frac{r^2}{2R} \left(\bar{R}'\Theta_{0,z} - \frac{I_{0,1}}{I_{2,0}}F(\Theta_0)\right),$$

so that expressions (4.7a) and (4.9a) imply that

$$\Delta_{r\phi}\Theta_1^* = 0, \quad \mathbf{x} \in \Omega, \quad t > 0, \quad (4.10a)$$

and the boundary condition (4.7b) gives

$$\frac{\partial\Theta_1^*}{\partial\mathbf{n}_{r\phi}} = \left[\left(1 + \frac{R_\phi^2}{R^2}\right)^{-1/2} \frac{R}{\bar{R}} \frac{I_{0,1}}{I_{2,0}} - 1\right] F(\Theta_0) = \alpha\lambda F(\Theta_0) + O(\alpha^2), \quad (4.10b)$$

where we have used (3.2a) and noted that the coefficient of  $\Theta_{0,z}$  vanishes identically. Motivated by the formal solution of (4.10a), we represent  $\Theta_1^*$  as

$$\Theta_1^*(r, \phi, z, t) = \Theta_1^a(z, t) + \alpha \sum_{k=1}^{\infty} r^k \theta_k(z, t) \cos(k\phi + d_k) + O(\alpha^2) \quad (4.11)$$

<sup>2</sup>Expression (4.9a) is valid for all  $\alpha$ . For weak anisotropy,  $I_{0,1}/I_{2,0} = 1 + O(\alpha^2)$ .

where  $\Theta_1^a(z, t) = \Theta_1(r = 0, z, t)$ . Computing the direction derivative of (4.11) at the boundary  $r = R(\phi, z)$  yields

$$\begin{aligned} \frac{\partial \Theta_1^*}{\partial \mathbf{n}_{r\phi}} &= \alpha \left(1 + \frac{R_\phi^2}{R^2}\right)^{-1/2} \sum_{k=1}^{\infty} k R^{k-1} \theta_k(z, t) \left(\cos(k\phi + d_k) + \frac{R_\phi}{R} \sin(k\phi + d_k)\right) \\ &= \alpha \sum_{k=1}^{\infty} k \bar{R}^{k-1} \theta_k(z, t) \cos(k\phi + d_k) + O(\alpha^2). \end{aligned} \quad (4.12)$$

Comparing (4.10b) with (4.12) implies that  $\theta_k$  is nontrivial only when  $k \in \{n_j\}_{j=1}^m$  and in these cases,  $d_k = \delta_k$ , and  $k \bar{R}^{k-1} \theta_k = \beta_k F(\Theta_0)$ . Finally,

$$\Theta_1(r, \phi, z, t) = \Theta_1^a(z, t) + r^2 \Theta_1^b(z, t) + \alpha \Theta_1^c(r, \phi, z, t) + O(\alpha^2) \quad (4.13a)$$

where, keeping only those terms to  $O(\alpha)$ ,

$$\Theta_1^b(z, t) = \frac{1}{2\bar{R}} (\bar{R}' \Theta_{0,z} - F(\Theta_0)), \quad (4.13b)$$

$$\Theta_1^c(r, \phi, z, t) = \bar{R} F(\Theta_0) \sum_{k=1}^m \frac{\beta_k}{n_k} \left(\frac{r}{\bar{R}}\right)^{n_k} \cos(n_k \phi + \delta_k). \quad (4.13c)$$

These last two terms are completely determined by  $\Theta_0$  and  $\bar{R}$ .

The derivation of the equations for  $\Theta_1^a(z, t)$  proceeds in a similar fashion as in the zeroth order model. In this case one uses (4.2) with  $j = 1$  and (4.3b) so that

$$\Delta_{r\phi} \Theta_2 = \frac{1}{\text{St}} \Theta_{1,t} - \Theta_{1,zz}, \quad \mathbf{x} \in \Omega, \quad t > 0, \quad (4.14a)$$

$$\frac{\partial \Theta_2}{\partial \mathbf{n}_{r\phi}} = -F'(\Theta_0) \Theta_1 + \frac{R_z \Theta_{1,z}}{\left(1 + \frac{R_\phi^2}{R^2}\right)^{1/2}} - \frac{1}{2} \frac{R_z^2 F(\Theta_0)}{\left(1 + \frac{R_\phi^2}{R^2}\right)}, \quad r = R(\phi, z). \quad (4.14b)$$

The compatibility condition and expression (4.13a) yield to  $O(\alpha)$

$$\begin{aligned} \frac{1}{\text{St}} \Theta_{1,t}^a &= \Theta_{1,zz}^a + \frac{2}{\bar{R}} (\bar{R}' \Theta_{1,z}^a - F(\Theta_0)) + 2\bar{R} (\bar{R}' \Theta_{1,z}^b - F(\Theta_0)) \\ &\quad - 2\bar{R}^2 \left[ \frac{\bar{R}'^2}{\bar{R}} F(\Theta_0) + \left( \frac{1}{\text{St}} \Theta_{1,t}^b - \Theta_{1,zz}^b \right) \right], \quad 0 < z < S_0(t), \quad t > 0 \end{aligned} \quad (4.15a)$$

where we note that  $\Theta_1^c$  in (4.13a) is removed by the angular integration. The boundary and initial conditions ((4.4b) and (4.5b) evaluated at  $r = 0$ ) read

$$\Theta_{1,z}^a(0, t) = \delta \Theta_1^a(0, t), \quad t \geq 0, \quad (4.15b)$$

$$\Theta_1^a(S_0(t), t) = -S_1(r = 0, t) \Theta_{0,z}(S_0(t), t), \quad t \geq 0. \quad (4.15c)$$

The time evolution of  $S_1(r, \phi, t)$  is governed by (4.6b) repeated here for convenience

$$S_{1,t}(r, \phi, t) = \left( \Theta_{1,z} + S_1 \Theta_{0,zz} + \frac{\Theta_{1,r}^2}{\Theta_{0,z}} + \frac{\Theta_{1,\phi}^2}{r^2 \Theta_{0,z}} \right) \Big|_{z=S_0(t)}, \quad S_1(r, \phi, 0) = 0, \quad (4.15d)$$

with  $\Theta_1$  given by (4.13).

**5. Thermal Stress for Isotropic Solids.** The thermal stress experienced by the crystal during its growth leads to the generation of structural defects in the crystal. To simplify the discussion, we use the plane strain assumption in this paper and in the following discussion the displacement vector is denoted by  $\mathbf{u} = (u^r, u^\phi)^T$  in polar co-ordinates generalizing the discussion in [2].

**5.1. Basic equations.** Consider a two-dimensional (plane strain) thermoelastic problem with displacement  $\mathbf{u}$  in polar coordinates. In this paper we will use the tensor and vector notations simultaneously, whenever it is convenient. By writing the stress tensor  $\sigma$  as

$$\sigma_{ij}^{\text{tot}} = \sigma_{ij} - \frac{E\alpha_0}{1-2\nu}(T - T_g)\delta_{ij}, \quad (5.1)$$

where  $\nu$ ,  $E$ , and  $\alpha_0$  are respectively, the Poisson ratio, Young's modulus, and coefficient of thermal expansion,  $\sigma_{ij}$  satisfies

$$\sigma_{ij} = \frac{E}{1+\nu} \left( e_{ij} + \frac{\nu}{1-2\nu} e_{kk} \delta_{ij} \right), \quad e_{kk} = e_{rr} + e_{\phi\phi}, \quad (5.2)$$

where the non-trivial strains satisfy

$$e_{rr} = \frac{\partial u^r}{\partial r}, \quad e_{r\phi} = \frac{1}{2} \left( \frac{\partial u^\phi}{\partial r} - \frac{u^\phi}{r} + \frac{1}{r} \frac{\partial u^r}{\partial \phi} \right), \quad e_{\phi\phi} = \frac{1}{r} \frac{\partial u^\phi}{\partial \phi} + \frac{u^r}{r}, \quad (5.3)$$

and the equations of thermoelastic equilibrium,  $\nabla \cdot \sigma^{\text{tot}} := \sigma_{ij,j}^{\text{tot}} = 0$ , take the form

$$\frac{\partial \sigma_{rr}}{\partial r} + \frac{1}{r} \frac{\partial \sigma_{r\phi}}{\partial \phi} + \frac{\sigma_{rr} - \sigma_{\phi\phi}}{r} = \frac{\alpha_0 \Delta T E}{1-2\nu} \frac{\partial \Delta \Theta}{\partial r}, \quad (5.4a)$$

$$\frac{\partial \sigma_{r\phi}}{\partial r} + \frac{1}{r} \frac{\partial \sigma_{\phi\phi}}{\partial \phi} + \frac{2\sigma_{r\phi}}{r} = \frac{\alpha_0 \Delta T E}{1-2\nu} \frac{1}{r} \frac{\partial \Delta \Theta}{\partial \phi}, \quad (5.4b)$$

where  $r < R(\phi, z)$  for  $0 < z < S(t)$  and  $\Delta T \Theta = T - T_g$ . By adopting the scaling in Section 3.2 for  $r$  and  $T$  in addition to

$$(u^r, u^\phi) = \tilde{R} \alpha_0 \Delta T (\hat{u}^r, \hat{u}^\phi), \quad \sigma_{ij} = \frac{\alpha_0 \Delta T E}{1-\nu} \hat{\sigma}_{ij}, \quad e_{ij} = \alpha_0 \Delta T \hat{e}_{ij}, \quad \phi = \hat{\phi},$$

equations (5.1) and (5.2) become, after dropping the hats for brevity,

$$\sigma_{ij}^{\text{tot}} = \sigma_{ij} - \frac{1-\nu}{1-2\nu} \Theta \delta_{ij}, \quad (5.5)$$

$$\sigma_{ij} = \frac{1-\nu}{1+\nu} \left( e_{ij} + \frac{\nu}{1-2\nu} e_{kk} \delta_{ij} \right). \quad (5.6)$$

The equations of thermoelastic equilibrium (5.4) become

$$\nabla \cdot \sigma = \mathbf{F} := \epsilon \frac{1-\nu}{1-2\nu} \nabla \Theta_1, \quad (5.7a)$$

or in component form

$$\frac{\partial \sigma_{rr}}{\partial r} + \frac{1}{r} \frac{\partial \sigma_{r\phi}}{\partial \phi} + \frac{\sigma_{rr} - \sigma_{\phi\phi}}{r} = \epsilon \frac{1-\nu}{1-2\nu} \frac{\partial \Theta_1}{\partial r}, \quad (5.7b)$$

$$\frac{\partial \sigma_{r\phi}}{\partial r} + \frac{1}{r} \frac{\partial \sigma_{\phi\phi}}{\partial \phi} + \frac{2\sigma_{r\phi}}{r} = \epsilon \frac{1-\nu}{1-2\nu} \frac{1}{r} \frac{\partial \Theta_1}{\partial \phi}. \quad (5.7c)$$

In the above expressions  $\Theta$  has been replaced by  $\epsilon\Theta_1$  which is the first nontrivial thermal contribution to the stress. Under the same scaling the stress free boundary condition on the surface  $r = R(\phi, z)$  with normal  $\mathbf{n}$  becomes

$$\boldsymbol{\sigma} \cdot \mathbf{n} = \mathbf{g} := \epsilon \frac{1-\nu}{1-2\nu} \Theta_1 \mathbf{n} \quad (5.8a)$$

which are (in component form)

$$\sigma_{rr} - \frac{R_\phi}{R} \sigma_{r\phi} = \epsilon \frac{1-\nu}{1-2\nu} \Theta_1, \quad r = R(\phi, z), \quad (5.8b)$$

$$\sigma_{r\phi} - \frac{R_\phi}{R} \sigma_{\phi\phi} = -\epsilon \frac{R_\phi}{R} \frac{1-\nu}{1-2\nu} \Theta_1, \quad r = R(\phi, z), \quad (5.8c)$$

where

$$\Theta_1(r, \phi, z, t) = \Theta_1^a(z, t) + r^2 \Theta_1^b(z, t) + \alpha \Theta_1^c(r, \phi, z, t) + O(\alpha^2).$$

A useful shorthand notation, especially in the anisotropic case, is to represent the non-dimensional versions of the strain-displacement (5.3) and stress-strain (5.6) relationships as

$$\mathbf{e} = \mathbf{S}(\mathbf{u}), \quad \boldsymbol{\sigma} = C_0 \mathbf{S}(\mathbf{u}) \quad (5.9)$$

respectively with the subscript zero on the stiffness matrix,  $C_0$ , indicating isotropy. By further defining the operators

$$\mathcal{L}_0 := \nabla \cdot C_0 \mathbf{S}, \quad \mathcal{B}_0 := C_0 \mathbf{S} \cdot \mathbf{n}, \quad (5.10)$$

the equilibrium equations (5.7) and boundary conditions (5.8) can be restated as the boundary value problem

$$\mathcal{L}_0(\mathbf{u}) = \mathbf{F}, \quad \mathbf{x} \in \Omega, \quad t > 0, \quad (5.11a)$$

$$\mathcal{B}_0(\mathbf{u}) = \mathbf{g}, \quad r = R(\phi, z). \quad (5.11b)$$

In practice, a complete set of solutions to (5.7) can be constructed with the Papkovitch-Neuber functions  $\Phi$ , and  $\Psi = (\psi_1, \psi_2)$  [3, 19]. These are based on the observation that provided  $\psi_1, \psi_2$  are harmonic and

$$\nabla(\Delta_{r\phi}\Phi) = \frac{(1+\nu)(1-2\nu)}{(1-\nu)^2} \mathbf{F}, \quad (5.12)$$

then a solution to (5.11) is given by the displacement vector

$$\mathbf{u} = \nabla(\Phi + \mathbf{r} \cdot \Psi) - 4(1-\nu)\Psi, \quad (5.13)$$

where  $\mathbf{r}$  is a position vector. The components of the stress tensor are found using (5.9).

**5.2. Perturbation solution of the thermoelastic equations.** Based on the assumption of  $\alpha \ll 1$ , we assume that the displacement has the following approximation:

$$\begin{aligned} u^r &\sim u_0^r + \alpha u_1^r + \alpha^2 u_2^r + \dots, \\ u^\phi &\sim u_0^\phi + \alpha u_1^\phi + \alpha^2 u_2^\phi + \dots. \end{aligned} \quad (5.14)$$

Applying (5.14) to (5.7) and expanding in powers of  $\alpha$  gives a sequence of approximations to the thermoelastic problem. In the following,  $\sigma_{ij}^n = \sigma_{ij}^n(u_n^r, u_n^\phi)$  denotes the components of the stress tensor generated by the displacement  $(u_n^r, u_n^\phi)$ . We find that  $\sigma_{ij}^0$  (analytically extended to  $r < \bar{R}(z)$ ) satisfy

$$\frac{\partial \sigma_{rr}^0}{\partial r} + \frac{1}{r} \frac{\partial \sigma_{r\phi}^0}{\partial \phi} + \frac{\sigma_{rr}^0 - \sigma_{\phi\phi}^0}{r} = 2\epsilon \frac{1-\nu}{1-2\nu} r \Theta_1^b, \quad r < \bar{R}(z), \quad (5.15a)$$

$$\frac{\partial \sigma_{r\phi}^0}{\partial r} + \frac{1}{r} \frac{\partial \sigma_{\phi\phi}^0}{\partial \phi} + \frac{2\sigma_{r\phi}^0}{r} = 0, \quad r < \bar{R}(z), \quad (5.15b)$$

with the boundary conditions

$$\sigma_{rr}^0 = \epsilon \frac{1-\nu}{1-2\nu} \bar{R}^2 \Theta_1^b, \quad r = \bar{R}(z), \quad (5.16a)$$

$$\sigma_{r\phi}^0 = 0, \quad r = \bar{R}(z). \quad (5.16b)$$

Solving for  $\sigma_{ij}^0$  we choose  $\epsilon \Theta_1 = \epsilon r^2 \Theta_1^b = f(r)$  in (5.12) so that

$$\Delta_{r\phi} \Phi = \frac{1+\nu}{1-\nu} (f(r) + A_0)$$

with  $A_0$  some constant to be determined. Setting  $\psi_1 = \psi_2 = 0$ , (5.13), and (5.16) give displacement components

$$\mathbf{u}_0 = \frac{1+\nu}{1-\nu} \frac{\epsilon r \Theta_1^b}{4} \begin{pmatrix} \bar{R}^2(1-2\nu) + r^2 \\ 0 \end{pmatrix} \quad (5.17)$$

as in [2]. Using (5.9) yields

$$\begin{pmatrix} \sigma_{rr}^0 \\ \sigma_{\phi\phi}^0 \\ \sigma_{r\phi}^0 \end{pmatrix} = \frac{1}{4} \epsilon \Theta_1^b \begin{pmatrix} \bar{R}^2 - r^2 \\ \bar{R}^2 - 3r^2 \\ 0 \end{pmatrix} + \epsilon \frac{1-\nu}{1-2\nu} r^2 \Theta_1^b \begin{pmatrix} 1 \\ 1 \\ 0 \end{pmatrix}. \quad (5.18)$$

In a similar fashion,  $\sigma_{ij}^1$  satisfy

$$\frac{\partial \sigma_{rr}^1}{\partial r} + \frac{1}{r} \frac{\partial \sigma_{r\phi}^1}{\partial \phi} + \frac{\sigma_{rr}^1 - \sigma_{\phi\phi}^1}{r} = \epsilon \frac{1-\nu}{1-2\nu} \frac{\partial \Theta_1^c}{\partial r}, \quad r < \bar{R}(z), \quad (5.19a)$$

$$\frac{\partial \sigma_{r\phi}^1}{\partial r} + \frac{1}{r} \frac{\partial \sigma_{\phi\phi}^1}{\partial \phi} + \frac{2\sigma_{r\phi}^1}{r} = \epsilon \frac{1-\nu}{1-2\nu} \frac{1}{r} \frac{\partial \Theta_1^c}{\partial \phi}, \quad r < \bar{R}(z), \quad (5.19b)$$

with the boundary conditions

$$\sigma_{rr}^1 - \lambda' \sigma_{r\phi}^0 + \lambda \bar{R} \frac{\partial \sigma_{rr}^0}{\partial r} = \epsilon \frac{1-\nu}{1-2\nu} \Theta_1^c + 2\lambda \epsilon \frac{1-\nu}{1-2\nu} \bar{R}^2 \Theta_1^b, \quad r = \bar{R}(z), \quad (5.20a)$$

$$\sigma_{r\phi}^1 - \lambda' \sigma_{\phi\phi}^0 + \lambda \bar{R} \frac{\partial \sigma_{r\phi}^0}{\partial r} = -\lambda' \epsilon \frac{1-\nu}{1-2\nu} \bar{R}^2 \Theta_1^b, \quad r = \bar{R}(z). \quad (5.20b)$$

To solve for  $\sigma_{ij}^1$  we first consider, without loss of generality, the  $k$ th component of  $\Theta_1^c$ . At this point it is convenient to introduce the notation  $(\mathcal{C}_k, \mathcal{S}_k) = (\cos(n_k \phi +$

$\delta_k$ ,  $\sin(n_k\phi + \delta_k)$ ) and the generalization  $(\tilde{\mathcal{C}}_k, \tilde{\mathcal{S}}_k)$  with  $\tilde{n}_k$  replacing  $n_k$ . In this notation (3.2) and (4.13) give

$$\lambda = \sum_{k=1}^m \beta_k \mathcal{C}_k, \quad \lambda' = - \sum_{k=1}^m \beta_k n_k \mathcal{S}_k, \quad \Theta_1^\epsilon = \bar{R}F(\Theta_0) \sum_{k=1}^m \frac{\beta_k}{n_k} \left(\frac{r}{\bar{R}}\right)^{n_k} \mathcal{C}_k. \quad (5.21)$$

Furthermore, using (5.18) to simplify (5.20),

$$\sigma_{rr}^1 = 2C_1\beta_k\mathcal{C}_k + 4\frac{1-\nu}{1-2\nu}\frac{C_2\beta_k}{n_k}\mathcal{C}_k, \quad r = \bar{R}(z), \quad (5.22a)$$

$$\sigma_{r\phi}^1 = 2C_1\beta_k n_k \mathcal{S}_k, \quad r = \bar{R}(z), \quad (5.22b)$$

where

$$C_1 = \frac{1}{4}\epsilon\bar{R}^2\Theta_1^b, \quad C_2 = \frac{1}{4}\epsilon\bar{R}F(\Theta_0). \quad (5.23)$$

We let  $\sigma_{ij}^1 = \sigma_{ij}^{1,p} + \sigma_{ij}^{1,h}$  where  $\sigma_{ij}^{1,p}$  is a particular solution of (5.19), and  $\sigma_{ij}^{1,h}$  is a homogeneous solution of (5.19) with a boundary condition that combines the particular solution and (5.22).

For  $\sigma_{ij}^{1,p}$ , setting  $\psi_1 = \psi_2 = 0$ , and choosing an appropriate  $\Phi$ , (5.13) yields the displacement

$$\mathbf{u}_{1,p} = \frac{1+\nu}{1-\nu} \frac{C_2\beta_k\bar{R}}{n_k(n_k+1)} \left(\frac{r}{\bar{R}}\right)^{n_k+1} \begin{pmatrix} (n_k+2)\mathcal{C}_k \\ -n_k\mathcal{S}_k \end{pmatrix}. \quad (5.24)$$

Using (5.9),

$$\begin{pmatrix} \sigma_{rr}^{1,p} \\ \sigma_{\phi\phi}^{1,p} \\ \sigma_{r\phi}^{1,p} \end{pmatrix} = C_2\beta_k \left(\frac{r}{\bar{R}}\right)^{n_k} \begin{pmatrix} \left(1 + \frac{2}{n_k(1-2\nu)}\right)\mathcal{C}_k \\ \left(-1 + \frac{2}{n_k(1-2\nu)}\right)\mathcal{C}_k \\ -\mathcal{S}_k \end{pmatrix}. \quad (5.25)$$

This leaves  $\sigma_{ij}^{1,h}$  which satisfies the homogeneous plate elasticity equation with boundary conditions

$$\sigma_{rr}^{1,h} = \left(2C_1 - \frac{(n_k-2)}{n_k}C_2\right)\beta_k\mathcal{C}_k, \quad r = \bar{R}(z), \quad (5.26a)$$

$$\sigma_{r\phi}^{1,h} = (2n_kC_1 + C_2)\beta_k\mathcal{S}_k, \quad r = \bar{R}(z). \quad (5.26b)$$

To match the boundary condition using (5.13) we combine  $\psi_1$  and  $\psi_2$  into a single harmonic function  $\Phi_1$ . To this end we choose  $\psi_1$  and  $\psi_2$  so that  $\nabla \cdot (\psi_1, -\psi_2) = 0$ . Assigning  $\nabla\Phi_1 = (\psi_1, -\psi_2)$ , implies  $\Delta\Phi_1 = 0$  provided  $\psi_1 = \Phi_{1,x}$ ,  $\psi_2 = -\Phi_{1,y}$ . Writing (5.13) in polar coordinates we find,

$$\mathbf{u}_{1,h} = \begin{pmatrix} \frac{\partial\Phi}{\partial r} \\ \frac{1}{r}\frac{\partial\Phi}{\partial\phi} \end{pmatrix} + (3-4\nu) \begin{pmatrix} -\frac{\partial\Phi_1}{\partial r} \cos 2\phi + \frac{\partial\Phi_1}{\partial\phi} \frac{\sin 2\phi}{r} \\ \frac{\partial\Phi_1}{\partial r} \sin 2\phi + \frac{\partial\Phi_1}{\partial\phi} \frac{\cos 2\phi}{r} \end{pmatrix} + r\mathbf{G} \quad (5.27)$$

where

$$\mathbf{G} = \begin{pmatrix} \frac{\partial^2\Phi_1}{\partial r^2} \cos^2\phi + \left(\frac{\partial\Phi_1}{\partial r} + \frac{1}{r}\frac{\partial^2\Phi_1}{\partial\phi^2}\right) \frac{\sin^2\phi}{r} - \left(\frac{\partial^2\Phi_1}{\partial r\partial\phi} - \frac{1}{r}\frac{\partial\Phi_1}{\partial\phi}\right) \frac{\sin 2\phi}{r} \\ \left(\frac{\partial^2\Phi_1}{\partial r^2} - \frac{1}{r}\frac{\partial\Phi_1}{\partial r} - \frac{1}{r^2}\frac{\partial^2\Phi_1}{\partial\phi^2}\right) \cos\phi \sin\phi + \left(\frac{\partial^2\Phi_1}{\partial r\partial\phi} - \frac{1}{r}\frac{\partial\Phi_1}{\partial\phi}\right) \frac{\cos 2\phi}{r} \end{pmatrix}.$$

By representing  $\Phi$  and  $\Phi_1$  as

$$\Phi_1(r, \phi) = \sum_{k=1}^{\infty} P_k r^k \cos(k\phi + a_k), \quad \Phi(r, \phi) = \sum_{k=1}^{\infty} Q_k r^k \cos(k\phi + b_k), \quad (5.28)$$

where  $P_k, Q_k, a_k,$  and  $b_k$  are arbitrary constants independent of  $r$  and  $\phi$ , expression (5.27) implies that

$$\mathbf{u}_{1,h} = \sum_{k=1}^{\infty} k r^{k-1} \begin{pmatrix} (k-4+4\nu)P_k \cos((k-2)\phi + a_k) + Q_k \cos(k\phi + b_k) \\ (4\nu - k - 2)P_k \sin((k-2)\phi + a_k) - Q_k \sin(k\phi + b_k) \end{pmatrix}. \quad (5.29)$$

Applying (5.9) once again yields

$$\begin{pmatrix} \sigma_{rr}^{1,h} \\ \sigma_{\phi\phi}^h \\ \sigma_{r\phi}^{1,h} \end{pmatrix} = \frac{1-\nu}{1+\nu} \sum_{k=1}^{\infty} k(k-1)r^{k-2} \begin{pmatrix} (k-4)P_k \cos((k-2)\phi + a_k) + Q_k \cos(k\phi + b_k) \\ -kP_k \cos((k-2)\phi + a_k) - Q_k \cos(k\phi + b_k) \\ (2-k)P_k \sin((k-2)\phi + a_k) - Q_k \sin(k\phi + b_k) \end{pmatrix}. \quad (5.30)$$

Imposing the boundary condition (5.26) we conclude that the only non-zero terms are associated with  $P_{n_k+2}, Q_{n_k}, a_{n_k+2}, b_{n_k}$  and  $a_{n_k+2} = b_{n_k} = \delta_k$ . Furthermore,  $P_{n_k+2}, Q_{n_k}$ , satisfy

$$\begin{pmatrix} (n_k+2)(n_k+1)(n_k-2) & n_k(n_k-1) \\ -(n_k+2)(n_k+1)n_k & -n_k(n_k-1) \end{pmatrix} \begin{pmatrix} \bar{R}_k^n P_{n_k+2} \\ \bar{R}_k^{n_k-2} Q_{n_k} \end{pmatrix} = \frac{1+\nu}{1-\nu} \beta_k \begin{pmatrix} 2C_1 - \frac{n_k-2}{n_k} C_2 \\ 2n_k C_1 + C_2 \end{pmatrix}$$

and on solving for  $P_{n_k+2}, Q_{n_k}$  we find

$$\begin{pmatrix} \sigma_{rr}^{1,h} \\ \sigma_{\phi\phi}^{1,h} \\ \sigma_{r\phi}^{1,h} \end{pmatrix} = \beta_k \begin{pmatrix} \left( \frac{n_k(n_k-1)C_1 r^{n_k-2}}{\bar{R}_k^{n_k-2}} + \frac{(n_k(n_k+1)C_1+C_2)(2-n_k)r^{n_k}}{n_k \bar{R}_k^{n_k}} \right) \mathcal{C}_k \\ \left( \frac{n_k(1-n_k)C_1 r^{n_k-2}}{\bar{R}_k^{n_k-2}} + \frac{(n_k(n_k+1)C_1+C_2)(n_k+2)r^{n_k}}{n_k \bar{R}_k^{n_k}} \right) \mathcal{C}_k \\ \left( \frac{n_k(1-n_k)C_1 r^{n_k-2}}{\bar{R}_k^{n_k-2}} + \frac{(n_k(n_k+1)C_1+C_2)r^{n_k}}{\bar{R}_k^{n_k}} \right) \mathcal{S}_k \end{pmatrix}. \quad (5.31)$$

The displacement is obtained by combining (5.17), (5.24) and (5.29) with restrictions on  $P_k, Q_k$  to yield

$$\mathbf{u}_0 + \alpha \mathbf{u}_1 = \begin{pmatrix} r D_r^{(1)} + r^3 D_r^{(3)} \\ 0 \end{pmatrix} + r^{n_k-1} \begin{pmatrix} D_r^- \mathcal{C}_k \\ D_\phi^- \mathcal{S}_k \end{pmatrix} + r^{n_k+1} \begin{pmatrix} D_r^+ \mathcal{C}_k \\ D_\phi^+ \mathcal{S}_k \end{pmatrix} \quad (5.32)$$

where

$$D_r^{(1)} = \left( \frac{1+\nu}{1-\nu} \right) C_1 (1-2\nu), \quad D_r^{(3)} = \left( \frac{1+\nu}{1-\nu} \right) \frac{C_1}{\bar{R}^2}, \quad (5.33a)$$

$$D_r^- = \left( \frac{1+\nu}{1-\nu} \right) \frac{C_1 \alpha \beta_k}{\bar{R}^{n_k-2}} n_k, \quad D_\phi^- = - \left( \frac{1+\nu}{1-\nu} \right) \frac{C_1 \alpha \beta_k}{\bar{R}^{n_k-2}} n_k, \quad (5.33b)$$

$$D_r^+ = \left( \frac{1+\nu}{1-\nu} \right) \frac{C_1 \alpha \beta_k}{\bar{R}^{n_k}} (2-4\nu - n_k) + \frac{4(1+\nu)}{n_k(n_k+1)} \frac{C_2 \alpha \beta_k}{\bar{R}^{n_k}}, \quad (5.33c)$$

$$D_\phi^+ = \left( \frac{1+\nu}{1-\nu} \right) \frac{C_1 \alpha \beta_k}{\bar{R}^{n_k}} (4-4\nu + n_k) + \frac{4(1+\nu)}{n_k(n_k+1)} \frac{C_2 \alpha \beta_k}{\bar{R}^{n_k}}. \quad (5.33d)$$

Combining (5.5), (5.18), (5.25), and (5.31) yields the components of the total stress

$$\begin{aligned} \begin{pmatrix} \sigma_{rr}^{\text{tot}} \\ \sigma_{\phi\phi}^{\text{tot}} \\ \sigma_{r\phi}^{\text{tot}} \end{pmatrix} &= C_1 \begin{pmatrix} 1 - \left(\frac{r}{R}\right)^2 \\ 1 - 3\left(\frac{r}{R}\right)^2 \\ 0 \end{pmatrix} + \alpha C_1 \beta_k n_k (n_k - 1) \left(\frac{r}{R}\right)^{n_k - 2} \begin{pmatrix} \mathcal{C}_k \\ -\mathcal{C}_k \\ -\mathcal{S}_k \end{pmatrix} \\ &+ \alpha C_1 \beta_k (n_k + 1) \left(\frac{r}{R}\right)^{n_k} \begin{pmatrix} (2 - n_k)\mathcal{C}_k \\ (n_k + 2)\mathcal{C}_k \\ n_k \mathcal{S}_k \end{pmatrix}. \end{aligned} \quad (5.34a)$$

Since  $e_{zz} = 0$ , the stress-strain relation (5.6) with (5.5) implies that

$$\sigma_{zz}^{\text{tot}} = \nu(\sigma_{rr}^{\text{tot}} + \sigma_{\phi\phi}^{\text{tot}}) - (1 - \nu)\epsilon\Theta_1.$$

Using (5.34a) gives

$$\sigma_{zz}^{\text{tot}} = 2C_1 \left(1 - 2\left(\frac{r}{R}\right)^2\right) + 4\alpha\beta_k \left(\nu(n_k + 1)C_1 - \frac{1 - \nu}{n_k}C_2\right) \left(\frac{r}{R}\right)^{n_k} \mathcal{C}_k \quad (5.34b)$$

where we have also added the quantity  $2C_1(1 - \nu)$ , using Saint Venant's principle, so that the average of  $\sigma_{zz}^{\text{tot}}$  over the surface  $A(z)$  is zero.

**5.3. The von Mises and total resolved stress.** A characteristic amount of stress can be assigned to each point with the von Mises stress which satisfies

$$\begin{aligned} 2\sigma_{\text{vm}}^2 &= (\sigma_1 - \sigma_2)^2 + (\sigma_1 - \sigma_3)^2 + (\sigma_2 - \sigma_3)^2 \\ &= (\sigma_{rr} - \sigma_{\phi\phi})^2 + (\sigma_{rr} - \sigma_{zz})^2 + (\sigma_{\phi\phi} - \sigma_{zz})^2 + 6\sigma_{r\phi}^2 \end{aligned} \quad (5.35)$$

where  $\sigma_1, \sigma_2, \sigma_3$  denote the eigenvalues of the stress tensor given by (5.34a).

The preferred method of dislocation generation in all III-V semiconductors, is through the generation of slip defects, in particular the  $\{111\}$ ,  $\langle 1\bar{1}0 \rangle$  slip system [2]. Consisting of four glide planes within which atoms can slip in one of three directions, the resolved stress  $\sigma_{\text{rs}}$ , in a particular slip direction  $\vec{g}$  within the glide plane with normal is given by

$$\sigma_{\text{rs}} = \vec{g}^T U_{\mathbf{p}}^T Q^T \sigma^{\text{tot}} Q U_{\mathbf{p}} \vec{n}.$$

The matrix  $U_{\mathbf{p}}$  rotates vectors from the crystallographic frame to the solidification frame so that for a given pulling direction, the rows of  $U_{\mathbf{p}}$  are the vectors  $\mathbf{a}$ ,  $\mathbf{b}$  and  $\mathbf{p}$ . If the stress tensor  $\sigma^{\text{tot}}$  is expressed in the  $(r, \phi, z)$  coordinates,  $Q$  is the coordinate transformation matrix that takes  $(x, y, z) \rightarrow (r, \phi, z)$ ,

Plastic deformation of the crystal occurs if the stress in any of the 12 slip directions exceeds a maximum value known as the critical resolved shear stress,  $\sigma_{\text{crss}}$ . To leading order, the actual density of dislocations suffered by the crystal is proportional to the total excess stress at any given point within the crystal. In this sense, an estimation of where dislocations are likely to occur is given by the distribution of the total absolute resolved stress

$$|\sigma_{\text{rs}}^{\text{tot}}| = \sum_{i=1}^{12} |\vec{g}_i^T U_{\mathbf{p}}^T Q^T \sigma^{\text{tot}} Q U_{\mathbf{p}} \vec{n}_i|. \quad (5.36)$$

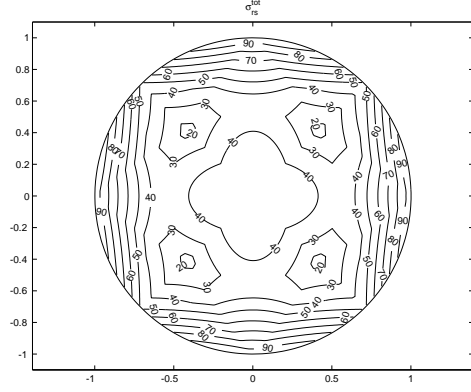


FIG. 6.1. Total resolved stress distribution just inside the crystal-melt interface at the end of the growth for a crystal pulled in the [001] direction. All reported stress values are expressed in percent with 100% occurring at the outer edge of a crystal grown in the [001] direction. For this orientation  $\max |\sigma_{rs}^{tot}| = 9.18 \times 10^{-3}$  and  $\min |\sigma_{rs}^{tot}| = 1.48 \times 10^{-3}$  corresponding to 0.975 MPa and 0.159 MPa respectively.

**6. Numerical Results.** The base geometry for the computation is a cone with  $1/2$  opening angle of  $\varphi_{\text{cone}} = 5^\circ$  so that  $\bar{R}(z) = \bar{R}(Z_0) + \alpha_{\text{cone}}z$ . We take  $Z_0 = 0.1$  and  $\bar{R}(Z_0) = 1/6$  corresponding to an initial dimensional seed radius and length of 0.005 m. The final radius and length is 0.0286 m and 0.3 m or 0.954 and 1 in non-dimensional units. This gives a value of  $\alpha_{\text{cone}} = 0.875$ .

For the thermal model,  $\Theta_0$  is the solution of (4.9) in the pseudo-steady case ( $1/\text{St} = 0$ ) with  $\delta = \gamma = 0$  and  $I_{0,1}/I_{2,0} = 1$ .  $\Theta_1$  is given by (4.13) with  $h_F = 0, h_{\text{gs}} = \bar{h}_{\text{gs}} = 1$  so that  $F(\Theta) = \beta\Theta = \Theta$ . Also,  $\Theta_1^c$  is defined by the data in Table 2.1,  $\Theta_1^b$  is derived from  $\Theta_0$  and  $\Theta_1^a$  satisfies (4.15). The Biot number is taken as  $\epsilon = 0.026$ .

We present the distribution of  $\sigma_{rs}^{\text{tot}}$  as given by (5.36) with the total stress given by (5.34). The values of  $E$  and  $\nu$  are chosen to be those associated with the  $\{111\}$  planes since these are invariant quantities for crystals with cubic symmetry [4] as well as being responsible for generating the slip defects within these crystals. These values are given by

$$E_{\{111\}} = \frac{4(C_{11} + 2C_{12})(C_{11} - C_{12})C_{44}}{(C_{11} + 2C_{12})(C_{11} - C_{12}) + 2C_{11}C_{44}} = 6.20 \times 10^4 \text{ MPa}, \quad (6.1a)$$

$$\nu_{\{111\}} = \frac{1}{3} \frac{(C_{11} + 2C_{12})(C_{11} - C_{12}) - 2C_{44}(C_{11} - 4C_{12})}{(C_{11} + 2C_{12})(C_{11} - C_{12}) + 2C_{11}C_{44}} = 0.362, \quad (6.1b)$$

where we have used the stiffness constants for InSb:  $C_{11} = 6.70 \times 10^4, C_{12} = 3.65 \times 10^4, C_{44} = 3.02 \times 10^4$  MPa. When combined with the parameters above, the dimensional constant for the stress calculations is  $\alpha_0 \Delta T E / (1 - \nu) \sim 106$  MPa.

In Figure 6.1, we plot the contours of the resolved stress for crystals pulled at the [001] direction. Since the cross-section is circular, the solution obtained previously in [2] applies. In Figures 6.2 and 6.3, we plotted the contours of the resolved stress for crystals grown by pulling the seeds in the  $[\bar{1}\bar{1}\bar{1}]$  and  $[\bar{2}11]$  directions, respectively. In both cases, stress is plotted for both circular and faceted cross-sections. As it can be seen from the plots, facet formation has a visible effect on the thermal stress inside these crystals. The maximum values of the stress are bigger in crystals with facets. In addition, higher stress levels are more concentrated close to the lateral surface for

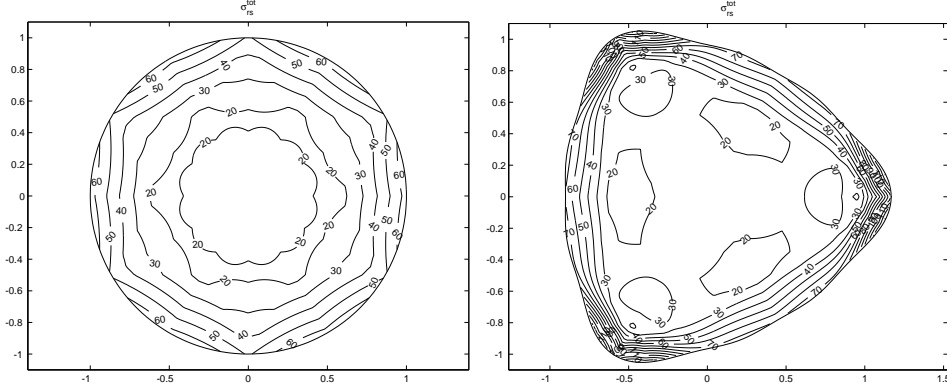


FIG. 6.2. Total resolved stress distribution just inside the crystal-melt interface at the end of the growth for a crystal pulled in the  $[\bar{1}\bar{1}\bar{1}]$  direction with and without facets. For this orientation  $\max|\sigma_{rs}^{tot}| = 13.1 \times 10^{-3}$  and  $\min|\sigma_{rs}^{tot}| = 1.19 \times 10^{-3}$  corresponding to 1.39 MPa and 0.126 MPa respectively.

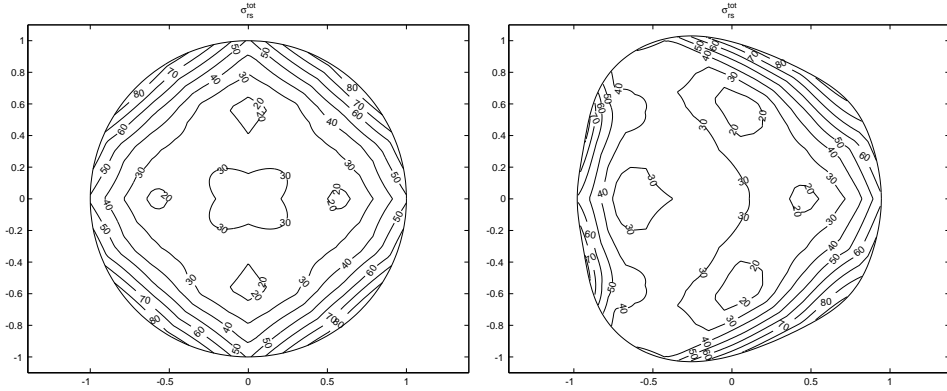


FIG. 6.3. Total resolved stress distribution just inside the crystal-melt interface at the end of the growth for a crystal pulled in the  $[\bar{2}11]$  direction with and without facets. For this orientation  $\max|\sigma_{rs}^{tot}| = 8.63 \times 10^{-3}$  and  $\min|\sigma_{rs}^{tot}| = 1.28 \times 10^{-3}$  corresponding to 0.916 MPa and 0.135 MPa respectively.

these crystals. Our results suggest that the axisymmetric calculation [2] may under predict the thermal stress for certain seed orientations.

Among the three seeding orientations considered in this study, the effect of facet formation on the stress is much stronger for the  $[\bar{1}\bar{1}\bar{1}]$  pulling direction than that for the  $[\bar{2}11]$  pulling direction. The  $[\bar{1}\bar{1}\bar{1}]$  direction not only produces higher stresses, but also a more extensive region of high stresses. Despite facet formation, the maximum stress for the  $[\bar{2}11]$  orientation is in fact lower than that for the  $[001]$  orientation without facets. These observation indicates that the  $[\bar{1}\bar{1}\bar{1}]$  orientation should be avoided while the  $[\bar{2}11]$  direction should be favored.

**7. Conclusion.** In this paper we propose a novel model to predict facet formation for constrained crystal growth such as the Czochralski process. The model used a simple argument based on the crystal lattice structure and facets are predicted for crystals in the  $[\bar{1}\bar{1}\bar{1}]$  and  $[\bar{2}11]$  seeding directions but not in the  $[001]$  direction, for a

given growth angle. Assuming that the anisotropic effect due to facet formation is weak, a domain perturbation method is used to derive thermal stress, as a generalization of the approach used in a previous study for axisymmetric crystals [2]. Numerical results show that facet formation greatly affects thermal stress distribution and defects are more likely to form in faceted crystals with certain seed orientations due to high stress levels while other orientations may be favored because of reduced stress levels.

**Acknowledgment.** The authors would like to acknowledge the support from NSERC (HH), MITACS (HH and JW), and Firebird Inc. (HH and CSB).

## REFERENCES

- [1] Anslanov, L.A. (1988). *Crystal-Chemical Model of Atomic Interactions to Hexagonal, Trigonal and Tetragonal Systems*. Acta Crystallographia: Series B, 44(5), pp. 458-462.
- [2] Bohun, C.S., Frigaard, Huang, H. & Liang, S. (2006). *A Semianalytical Thermal Stress Model for the Czochralski Growth of Type III-V Compounds*. SIAM Journal of Applied Mathematics, 66(5), pp. 1533-1562.
- [3] Boley, B.A & Weiner, J.H. (1997). *Theory of Thermal Stresses*, 3rd. ed. Dover Publications: New York.
- [4] Brantley, W.A. (1973). *Calculated elastic constraints for stress problems associated with semiconductor devices*. Journal of Applied Physics, 44(1), pp. 534-535.
- [5] Brattkus, K. & Davis, S.H. (1988). *Directional solidification with heat losses*. Journal of Crystal Growth, 91(4), pp. 538-556.
- [6] Chen, T., Wu, H. & Weng, C. (1997). *The effect of interface shape on anisotropic thermal stress of bulk single crystal during Czochralski growth*. Journal of Crystal Growth, 173(3-4), pp. 367-379.
- [7] Chieh, C. (1979). *The Archimedean Truncated Octahedron, and Packing of Geometric Units in Cubic Crystal Structures*. Acta Crystallographia: Series A, 35(6), pp. 946-952.
- [8] Davis S.H. (2001). *Theory of Solidification*, Cambridge University Press.
- [9] Golovin, A.A. & Davis, S.H. (1998). *Effect of Anisotropy on Morphological Instability in the Freezing of a Hypercooled Melt*. Physica D, 161, pp. 363-391.
- [10] Hariharan, S.I. & Young, G.W. (2001). *Comparison of asymptotic solutions of a phase-field model to a sharp-interface model*. SIAM Journal of Applied Mathematics, 62(1), pp. 244-263.
- [11] Hartman, P. & Perdok, W.G. (1955). *On the Relations Between Structure and Morphology of Crystals. III*. Acta Crystallographica, 8(9), pp. 525-529.
- [12] Hoyle, R.B., McFadden, G.B. & Davis, S.H. (1996). *Pattern Selection with Anisotropy during Directional Solidification*. Proc. Royal Soc. Lond, A 354, pp. 2915-2949.
- [13] Kuiken, H.K. & Roksnoer, P.J. (1979). *Analysis of the temperature distribution in FZ silicon crystals*. Journal of Crystal Growth, 47(1), pp. 29-42.
- [14] Li, W., Shi, E., Zhong, W. & Yin, Z. (1999). *Growth mechanism and growth habit of oxide crystals*. Journal of Crystal Growth, 203(1-2), pp. 186-196.
- [15] Li, W., Shi, E., Zhong, W. & Yin, Z. (1999). *Anion coordination polyhedron growth unit: theory, model and crystal morphology*. Journal of Synthetic Crystals, 28(2), pp. 117-125.
- [16] Li, W., Shi, E., Chen, Z. & Yin, Z. (2000). *Growth habit of polar crystals*. Chinese Science Bulletin, 45(18), pp. 1662-1666.
- [17] Li, W., Shi, E., Chen, Z. & Yin, Z. (2001). *Coordination polyhedron growth mechanism model and growth habit of crystals*. Science in China: Series B, 44(2), pp. 123-136.
- [18] Micklethwaite, W.F.H. (2005). *The Bulk Growth of InSb & Related Ternary Alloys*. In *Bulk Crystal Growth of Electronic, Optical and Optoelectronic Materials*, Chapter 5, Capper, P. ed., John Wiley & Sons: New Jersey.
- [19] Mindlin, R. (1936). *Note on the Galerkin and Papkovitch stress functions*. Bulletin of the American Mathematics Society, 42, pp. 373-376.
- [20] Miyazaki, N. (2002). *Development of a thermal stress analysis system for anisotropic single crystal growth*. Journal of Crystal Growth, 236(1-3), pp. 455-465.
- [21] O'Keeffe, M. (1978). *Non-Bonded Interactions and the Crystal Chemistry of Tetrahedral Structures Related to the Wurtzite Type (B<sub>4</sub>)*. Acta Crystallographia: Series B, 34(12), pp. 3519-3528.
- [22] Parthé, E & Engel, N. (1986). *Relation Between Tetrahedron Connections and Composition*

- for Structures with Tetrahedral Anion Complexes. *Acta Crystallographia: Series B*, 42(6), pp. 538-544.
- [23] Parthé, E & Chabot, B. (1990). *Classification of Structures with Anionic Tetrahedron Complexes using Valence-Electron Criteria*. *Acta Crystallographia: Series B*, 46(1), pp. 7-23.
- [24] Pet'kov, I.S. & Red'kin, B.S. (1993). *Calculation of the stationary cross-section form of non-axisymmetrical crystals growing from the melt*. *Journal of Crystal Growth*, 131(3-4), pp. 598-606.
- [25] Russo, G. & Smereka, P. (2000). *A level-set method for the evolution of faceted crystals*. *SIAM Journal on Scientific Computing*, 21(6), pp. 2073-2095.
- [26] Vigdergauz, S. & Givoli, D. (1999). *Thermoelastic stresses in a crystal with weak anisotropy*. *Journal of Crystal Growth*, 198-199(part 1), pp. 125-128.
- [27] Vigdergauz, S. & Givoli, D. (1999). *Thermoelastic stresses in a cylinder or disk with cubic anisotropy*. *International Journal of Solids and Structures*, 36(14), pp. 2109-2125.
- [28] Wu, J.-B., Bohun, C.S. & Huang, H. (2007). *A Thermal Elastic Model for Directional Crystal Growth with Weak Anisotropy*, submitted.
- [29] Young, G.W., & Chait, A. (1990). *Surface tension driven heat, mass, and momentum transport in a two-dimensional float-zone*. *Journal of Crystal Growth*, 106(2-3), pp. 445-466.
- [30] Young, G.W. & Heminger, J.A. (1997). *Modeling the time-dependent growth of single-crystal fibers*. *Journal of Crystal Growth*, 178(3), pp. 410-421.
- [31] Young, G.W. & Heminger, J.A. (2000). *A mathematical model of the edge-defined film-fed growth process*. *Journal of Engineering Mathematics*, 38, pp. 371-390.
- [32] Yuan, R., Shi, E., Li, W., Zheng, Y., Wu, N. & Zhong, W. (2000). *The growth units and hydrothermal preparation of lead tungstate (PbWO<sub>4</sub>) crystallites*. *Science in China: Series E*, 43(5), pp. 495-503.
- [33] Zhang, X., Luo, H. & Zhong, W. (2004). *Growth unit model of anion coordination-polyhedra and its application to crystal growth*. *Science in China: Series E*, 47(2), pp. 191-202.
- [34] Zhong, W., Liu, G. & Shi, E. (1994). *Growth unit and formation mechanisms of crystals under hydrothermal conditions*. *Science in China: Series B*, 37(11), pp. 1288-1291.
- [35] Zhong, W. & Tang, D. (1996). *Growth units and morphology of lithium tetraborate (LBO) crystals*. *Journal of Crystal Growth*, 166(1-4), pp. 91-98.